2007 IEEE International Conference on
Robotics and Automation
Roma, Italy, 10-14 April 2007

Image-guided Control of Flexible Bevel-Tip Needles

Vinutha Kallem Noah J. Cowan

Abstract— **Physicians perform percutaneous therapies in many diagnostic and therapeutic procedures. Image guidance promises to improve targeting accuracy and broaden the scope of needle interventions. In this paper, we consider the possibility of automating the guidance of a flexible bevel-tip needle as it is inserted into human tissue. We build upon a previously proposed nonholonomic kinematic model to develop a nonlinear observer-based controller. As a first step for control, we show that flexible needles can be automatically controlled to remain within a planar slice of tissue as they are inserted by a physician; our approach keeps the physician in the loop to control insertion speed. In the proposed controller, the distance of the needle tip position from the plane of interest is used as a feedback signal. Numerical simulations demonstrate the stability and robustness of the controller in the face of parametric uncertainty. We also present results from pilot physical experiments with phantom tissue under stereo image guidance.**

I. Introduction

Many diagnostic and therapeutic procedures require accurate needle targeting. In interventional brachytherapy for cancer treatment, a physician inserts a long thin needle into human tissue, guides it to the target where the seeds are to be placed, and then delivers the treatment. In fine needle aspiration biopsy and needle core biopsy, needles are used to access a designated area to remove a small amount of tissue from a lesion to test whether the tumor is malignant or benign. These techniques are based on medical images, relying on online fluoroscopy, ultrasound scanning, or prior MRI/CT scans of the targeted region. In many cases, a physician's performance is limited by the amount of "steering" she can obtain once the needle is inserted. Studies have shown that needle divergence from a desired path decreases effectiveness in both brachytherapy [11] and biopsy [2]. Efforts to overcome this have focused on improving imaging modalities for building pre- and intraoperative models, better path planning, and new needle placement devices.

Another approach to improving accuracy, and expanding the applicability of needle interventions in general, involves actively steering a needle as it is inserted into tissue. For a human operator, navigation in 3D under image guidance by manipulating the needle at the base would require profound spatial reasoning skills and extensive training even for the most skilled surgeon.

We propose the use of automatic control to enable real-time image-based following of pre-planned needle trajectories. Recent studies have presented and experimentally validated "plant models" for manipulating a needle from outside the patient. DiMaio and Salcudean [4] showed that symmetric tip needles that are stiff relative to the surrounding tissue can be steered by moving the base of the needle so as to deflect the tissue as the needle is inserted. They show that this effect can be modeled as a kinematic control system with a numerically determined Jacobian matrix that relates base motions to needle-tip motions. Glozman and Shoham [9] approximate the tissue using springs to compute local deformations for planning needle steering. Webster *et al.* consider flexible bevel-tip needles that do not significantly deflect surrounding tissue as they are inserted [13]. They model such needle insertion as a nonholonomic, kinematic control system. In both the rigid and flexible cases described above, the inputs at the base of needle can be treated as the input to a kinematic control system. While we know of no prior work on automatic image-guided needle steering control, path planning and obstacle avoidance have been investigated for both rigid [3], [5] and flexible needles [1], [12].

In the current paper, we design and demonstrate a nonlinear image-based observer-controller pair to stabilize a flexible bevel-tip needle to a desired 2D plane. We base our plant model on the nonholonomic kinematic model presented in [13]. We assume that the position of the needle tip can be measured by an imaging modality such as fluoroscopy or 3D ultrasound. This controller can serve as a low-level controller while implementing the 2D path planning algorithms developed in [1]. We believe that this step will also help us gain significant understanding of the control issues in a more generic path-following case.

II. System Overview and Needle Steering Model

A flexible bevel-tip needle [7], [8], [13] is one which can be steered by rotation and insertion at the base of the needle (outside the patient). The asymmetry of the bevel creates a moment at the needle tip, deflecting the needle and causing it to follow a circular arc. As the needle is rotated, the bevel tip is reoriented in space, so that subsequent insertion follows an arc in a new plane. Figure 1 shows a fluoroscope image of a needle being inserted into bovine muscle. It is clear that the flexible bevel-tip needle curves when inserted into tissue.

We have implemented a setup similar to that described in [13] which enables image-guided needle placement experiments (see Figure 2). We use transparent gels made from mixtures of PVC plastics, which have similar mechanical properties to human tissue. The insertion device has the ability to push the needle forward and to rotate the needle about its shaft and we treat the insertion and rotation speeds

V. Kallem and N. J. Cowan are with the Department of Mechanical Engineering, Johns Hopkins University, Baltimore, MD 21218 USA (e-mail: vkallem@jhu.edu, ncowan@jhu.edu).

1-4244-0602-1/07/$20.00 ©2007 IEEE.

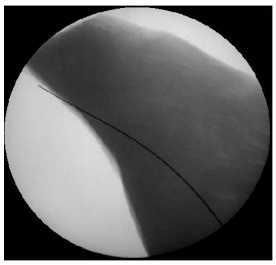

Fig. 1. This fluoroscope image demonstrates that a 0.6 mm diameter bevel tip nitinol needle can steer through bovine muscle [13].

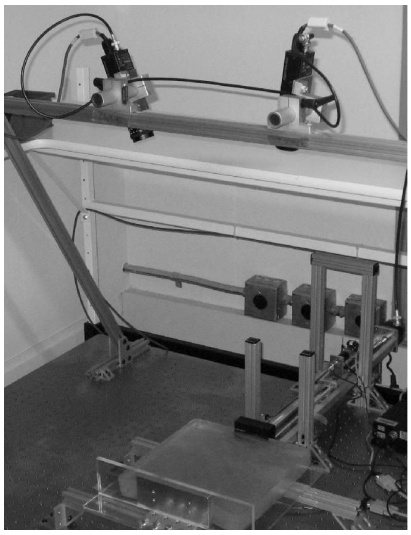

Fig. 2. The needle steering device inserts the needle into phantom tissue while the needle tip position is tracked using two overhead cameras.

as two inputs to a control system. Two overhead cameras track the needle as it is inserted through the gel.

As the needle is pushed through tissue, there is a small amount of tissue deformation and the needle must be steered to avoid bones and other sensitive organs through which it cannot or should not pass. Researchers have developed simulation-based path planning algorithms that compute an optimal path in the tissue while compensating for tissue deformations and avoiding obstacles. Alterovitz *et al.* currently have planning algorithms to generate desired needle trajectories within a 2D plane [1]. The output of these 2D planners is a path that can be followed by alternating between forward insertion of the needle in to the tissue without any rotation and a 180° rotation of the needle base without any insertion. This planner assumes that during the whole process, the needle stays in a known (nominal) 2D plane. However, our numerical tests (see Section V) indicate that small errors of only a few degrees in needle tip orientation cause the needle to deviate rapidly from the nominal 2D plane.

Planned trajectories have to be followed despite real world uncertainties such as noisy sensors, imperfect actuators, and small tissue deformations. In this current work we study the possibility of controlling the needle to stay in a desired

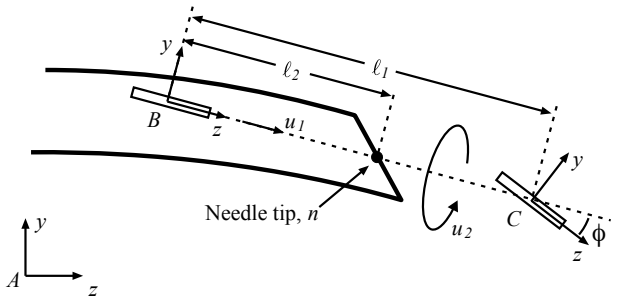

Fig. 3. Kinematic bicycle model: Frame A is the inertial world reference frame. Frames B and C are attached to the two wheels of the bicycle. This figure is reproduced from [13] with permission from the authors.

2D plane. We envision this controller can work in parallel with the 2D planners previously developed [1]. Whenever there is a 180° rotation, this controller can be employed to make the needle stay on the nominal plane, thus making the planning algorithm work. We believe that this work is a crucial first step in making inroads towards fully automated needle guidance in human tissue. Our controller will also allow us to validate the efficacy of the kinematic model described in [13].

We use the notation and kinematic model developed by Webster *et al.* [13] for a bevel tip flexible needle. It is modeled as a generalization of the nonholonomic bicycle model, and neglects torsional compliance of the needle shaft. This model (Figure 3) is reproduced here for reader convenience.

In the model, ℓ_1, ℓ_2 determine the location of bicycle wheels with respect to the needle tip. Parameter ϕ is the fixed front wheel angle relative to the rear wheel. Frame A is the inertial world reference frame and frames B and C are attached to the two wheels of the bicycle. In homogeneous coordinates, the rigid body transformation between frames A and B is given by the rigid body transformation matrix:

$$g = \begin{bmatrix} R & p \\ 0^T & 1 \end{bmatrix} \in \mathrm{SE}(3) \quad \text{where} \quad R \in \mathrm{SO}(3) \text{ and } \boldsymbol{p} \in \mathbb{R}^3.$$

Let $\boldsymbol{v}, \boldsymbol{\omega} \in \mathbb{R}^3$ denote, respectively, the linear and angular velocities of the needle tip written relative to frame A. Webster *et al.* use Lie-group theory to find a "coordinate-free" differential kinematic model:

$$\begin{bmatrix} \boldsymbol{v} \\ \boldsymbol{\omega} \end{bmatrix} = (g^{-1}g)^\vee = u_1 \mathbf{V}_1 + u_2 \mathbf{V}_2, \tag{1}$$

where $\hat{}$ and $^\vee$ are the usual isomorphism between $\mathfrak{se}(3)$ and $\mathbb{R}^6$, u_1 is the insertion speed, u_2 is the rotation speed of the needle, and the control vector fields are given by $\mathbf{V}_1 = [0, 0, 1, \kappa, 0, 0]^T$ (which corresponds to insertion) and $\mathbf{V}_2 = [0, \ldots, 0, 1]^T$ (which corresponds to needle rotation). Here, $\kappa = \tan\phi/\ell_1$ is the curvature that the needle follows. Note that insertion, u_1, causes the needle to move in the body-frame z-axis direction, but also to rotate (due to the bevel tip) about the body-frame x-axis. Rotation of the needle shaft, u_2, causes pure rotation of the needle tip about the z-axis.

III. Plant Model

We use Z-Y-X fixed angles as generalized coordinates to parameterize R, the rotation matrix between frames A and B. Let γ be the roll of the needle, β be the pitch of the needle out of the plane and α be the yaw of the needle in the plane. Let the position of the origin of frame B be $\boldsymbol{p} = [x, y, z]^T \in \mathbb{R}^3$ relative to the inertial frame A. We assume that an imaging system measures the location of the origin of frame B. Note that by driving the origin of frame B to the y-z plane the needle tip will also be stabilized to the y-z plane.

Using this notation, $\boldsymbol{q} = \left[x, y, z, \alpha, \beta, \gamma\right]^T \in \mathcal{U} \subset \mathbb{R}^6$ forms a (local) set of generalized coordinates for the configuration of the needle tip. The coordinates are well defined on

$$\mathcal{U} = \big\{[x, y, z, \alpha, \beta, \gamma]^T \in \mathbb{R}^6 : \alpha, \gamma \in \mathbb{R} \bmod 2\pi, \quad \beta \in (-\pi/2, \pi/2)\big\}. \tag{2}$$

It is easy to show that the body frame velocity may be expressed as

$$\mathbf{V} = J\dot{\boldsymbol{q}}, \text{ where}$$

$$J = \begin{bmatrix} R^T & 0_{3\times3} \\ 0_{3\times3} & A \end{bmatrix} \text{ and } A = \begin{bmatrix} \cos\beta\cos\gamma & \sin\gamma & 0 \\ -\cos\beta\sin\gamma & \cos\gamma & 0 \\ \sin\beta & 0 & 1 \end{bmatrix}.$$

and the kinematic model (1) of the bevel tip flexible needle reduces to

$$\dot{\boldsymbol{q}} = J^{-1}\mathbf{V}_1 u_1 + J^{-1}\mathbf{V}_2 u_2 = \begin{bmatrix} \sin\beta & 0 \\ -\cos\beta\sin\alpha & 0 \\ \cos\alpha\cos\beta & 0 \\ \kappa\cos\gamma\sec\beta & 0 \\ \kappa\sin\gamma & 0 \\ -\kappa\cos\gamma\tan\beta & 1 \end{bmatrix} \begin{bmatrix} u_1 \\ u_2 \end{bmatrix}. \tag{3}$$

Due to the introduction of generalized coordinates, there are singularities at $\beta = \pm\pi/2$ that cause $\det J = \cos\beta = 0$.

To stabilize the needle to the y-z plane, the states y, z, and α need not be controlled. Also, these states do not affect the dynamics of the remaining states, x, β, and γ. Let $\mathbf{x} = [x_1, x_2, x_3]^T = [x, \beta, \gamma]^T$ denote the state vector of the "reduced" order system. Tracking the needle tip with an imaging systems typically enable us to measure only the position of the needle and not its orientation (without performing any differentiation), which in reduced coordinates is just the distance from the y-z plane, namely x. This system can be represented in state space form:

$$\begin{aligned} \dot{\mathbf{x}} &= f(\mathbf{x})u_1 + g(\mathbf{x})u_2 = \begin{bmatrix} \sin x_2 \\ \kappa\sin x_3 \\ -\kappa\cos x_3\tan x_2 \end{bmatrix} u_1 + \begin{bmatrix} 0 \\ 0 \\ 1 \end{bmatrix} u_2 \\ \mathbf{y} &= h(\mathbf{x}) = x_1. \end{aligned} \tag{4}$$

Note that $\mathbf{x} = 0$ corresponds to the desired equilibrium state of remaining within the y-z plane to which we wish to stabilize the needle.

We reparameterize the system in terms of insertion distance, l, enabling the physician to control the insertion speed. In a slight abuse of notation, we write $\dot{\mathbf{x}}$ where we mean $d\mathbf{x}/dl$, and interpret the insertion distance as "time" for convenience of exposition.[1] This results in

$$\begin{aligned} \dot{\mathbf{x}} &= \begin{bmatrix} \sin x_2 \\ \kappa\sin x_3 \\ -\kappa\cos x_3\tan x_2 \end{bmatrix} + \begin{bmatrix} 0 \\ 0 \\ 1 \end{bmatrix} u \\ \mathbf{y} &= h(\mathbf{x}) = x_1, \text{ where } u = u_2/u_1. \end{aligned} \tag{5}$$

IV. Feedback Control

Using judiciously chosen generalized coordinates, we reduced the plant model to a third order nonlinear system (5). This system can be feedback linearized (see, e.g. [10]) via a transformation of state and input coordinates:

$$\begin{aligned} \mathbf{z} &= \left[h, L_f h, L_f^2 h\right]^T \\ &= \left[x_1, \quad \sin x_2, \quad \kappa\cos x_2 \sin x_3\right]^T \end{aligned} \tag{6}$$

and

$$v = L_f^3 h + L_g L_f^2 h u = -\kappa^2 \sin x_2 + \kappa\cos x_2\cos x_3 u. \tag{7}$$

The state equations in the feedback linearized form are:

$$\begin{aligned} \dot{\mathbf{z}} &= A_f\mathbf{z} + B_f v = \begin{bmatrix} 0 & 1 & 0 \\ 0 & 0 & 1 \\ 0 & 0 & 0 \end{bmatrix} \mathbf{z} + \begin{bmatrix} 0 \\ 0 \\ 1 \end{bmatrix} v \\ \mathbf{y} &= C_f\mathbf{z} = \begin{bmatrix} 1 & 0 & 0 \end{bmatrix} \mathbf{z}. \end{aligned} \tag{8}$$

The system (A_f, B_f, C_f) is completely controllable and observable.

A. Estimator Dynamics and Control

Note that even though the change of coordinates from the nonlinear system (5) to the feedback linearized system (8) is highly nonlinear, the first state – and more importantly the *output* – is identical for both systems. In other words the system is completely observable even though only one of the states ($\mathbf{y} = z_1 = x_1$) can be measured directly.

Hence, simple control system design techniques from linear system theory can be used to control this system. A full state Luenberger observer with the following dynamics estimates all the states from the output:

$$\begin{aligned} \dot{\hat{\mathbf{z}}} &= A_f\hat{\mathbf{z}} + B_f v + L(y - \hat{y}) \\ \hat{\mathbf{y}} &= C_f\hat{\mathbf{z}} = \begin{bmatrix} 1 & 0 & 0 \end{bmatrix} \mathbf{z}. \end{aligned} \tag{9}$$

The control input to the system is then given by full-state feedback, using the state estimate:

$$v = -K\hat{\mathbf{z}}. \tag{10}$$

Because the system is linear and time-invariant, the separability principle allows us to select the observer gain matrix, L, and proportional gain matrix, K, independently. Since estimates of the states are used to calculate the control input, u, we use high gain observer feedback. Note that it may be possible to measure the state x_2 too if the needle can be segmented while it is being inserted into the tissue. The

[1] This is equivalent to setting $u_1 = 1$ in (4).

"roll" (x_3) cannot be measured even in these cases due to very small size of the bevel-tip. In such cases, we can use a reduced state Luenberger observer instead of the full state observer.

Note that one difficulty arises because we must compute u from (7). However, we do not know $\mathbf{x}$, so we must use $\hat{\mathbf{z}}$ to compute an *estimate* of $\mathbf{x}$ by plugging $\hat{\mathbf{z}}$ into the inverse of (6). This implies that the estimator dynamics will have an input error. In this paper, we assume that the error computing u is negligible; determining the robustness of our observer-controller framework given this discrepancy is work in progress.

B. Stability Analysis

In the present framework, there are singularities at $\beta = \pm\pi/2$ due to the introduction of generalized coordinates. In addition, the nonlinear transformation from $\mathbf{x}$ to $\mathbf{z}$ also introduces singularities at $\gamma = \pm\pi/2$. This limitation seems inescapable: global linearization is mathematically impossible for dynamical systems on the space of rigid transformations. Fortunately, our feedback linearization scheme works for all needle positions and orientations except when the needle is orthogonal to the plane to which we are trying to stabilize. We believe that this scenario is not of clinical significance; such large errors in orientation should be addressed at the level of planning, not with low-level servo control.

That said, it is important for the above described controller never to take the system – or even the state estimate! – to these singularities. In this section, we perform Lyapunov stability analysis to find the region of attraction of the controller.

Let $r \in \mathbb{R}$ be a number such that $r < \frac{1}{2}\min(1, 1/\kappa)$. For $\mathbf{z} \in \mathcal{D} = \{\mathbf{z} \in \mathbb{R}^3 : \|\mathbf{z}\| \leq 2r\}$, the coordinate transformation mapping $\mathbf{x}$ to $\mathbf{z}$ is well-defined and invertible. This implies that β and γ never reach the singularities at $\pm\pi/2$. By defining $\mathbf{e} = \mathbf{z} - \hat{\mathbf{z}}$ as the error in estimation, the closed-loop feedback system is now given by

$$\begin{bmatrix}\dot{\mathbf{z}} \\ \dot{\mathbf{e}}\end{bmatrix} = \begin{bmatrix}A_f - B_f K & B_f K \\ A_f - LC_f & 0\end{bmatrix}\begin{bmatrix}\mathbf{z} \\ \mathbf{e}\end{bmatrix}.$$

The matrices K and L are chosen to make $(A_f - B_f K)$ and $(A_f - LC_f)$ Hurwitz (eigenvalues in the open left-half plane). Hence for every such K and L, there exist real symmetric positive definite matrices P and R such that $(A_f - B_f K)^T P + P(A_f - B_f K) = -I$ and $(A_f - LC_f)^T R + R(A_f - LC_f) = -I$, respectively. Consider the sets $D_e = \{\mathbf{e} \in \mathbb{R}^3 : \|\mathbf{e}\| \leq r\}$ and $D_z = \{\mathbf{z} \in \mathbb{R}^3 : \|\mathbf{z}\| \leq r\}$. We define a positive definite function $V : D_z \times D_e \to \mathbb{R}$ as:

$$V(\mathbf{z}, \mathbf{e}) = a\mathbf{z}^T P \mathbf{z} + b\mathbf{e}^T R \mathbf{e} \text{ where } a, b \in \mathbb{R}, a, b > 0.$$

Taking the time derivative of the function V, we obtain

$$\begin{aligned}\dot{V}(\mathbf{z}, \mathbf{e}) &= -a\mathbf{z}^T\mathbf{z} - b\mathbf{e}^T\mathbf{e} + 2a\mathbf{z}^T P B_f K \mathbf{e} \\ &= -a\left\|\mathbf{z} - PB_f K\mathbf{e}\right\|^2 - b\left\|\mathbf{e}\right\|^2 \\ &\quad + a\mathbf{e}^T(K^T B_f^T P^2 B_f K)\mathbf{e}\end{aligned}$$

Note that $Q = K^T B_f^T P^2 B_f K$ is a real symmetric positive semi-definite matrix. Hence we can always choose $a, b \in R$ and $a, b > 0$ with $b > a\lambda_{max}(Q)$. With this choice of a and b, we observe that V is a Lyapunov function for the complete closed-loop feedback system.

Our goal is to ensure that neither the states, nor their estimates, encounter the singularities introduced by feedback linearization. Note that

$$V \geq \lambda_{min}(P)\left\|\mathbf{z}\right\|^2 + \lambda_{min}(R)\left\|\mathbf{e}\right\|^2 \geq d\left\|\mathbf{z}\right\|^2 + d\left\|\mathbf{e}\right\|^2,$$

where $d = \min(\lambda_{min}(P), \lambda_{min}(R))$. If $c > 0 \in \mathbb{R}$ is chosen such that $c \leq dr^2$, then for all $(\mathbf{z}, \mathbf{e}) \in S = \{(\mathbf{z}, \mathbf{e}) \in D_z \times D_e : V(\mathbf{z}, \mathbf{e}) \leq c\}$, $\mathbf{z}, \hat{\mathbf{z}}$ belongs to the set D. If the initial deviation of the system from the desired plane is such that the initial states are in S, then the proposed controller will stabilize the needle to the desired plane without reaching any singularities.

V. Experimental Validation

A. Numerical Simulations

Extensive simulations were conducted in MATLAB to test our proposed controller. We used a discrete-time implementation of the system and the controller-observer pair, to reflect a real-world implementation as closely as possible. The plant model was discretized assuming constant insertion of the needle into the tissue between samples. We assumed measurement noise of up to ± 1 mm with a uniform distribution. This seems clinically reasonable given that 3D ultrasound imaging can be accurate to within 0.8 mm [6]. The parameter value for the model has been taken to be $1/\kappa = 9.7\ cm$, the smallest radius of curvature value we have achieved in laboratory trials.

In our simulations, it was observed that if the entry point is too far away from the desired plane, the estimator states leave the region of attraction. To avoid such singularities, we performed estimator saturation, i.e., if the estimator states left the region of attraction, they were pulled back to the closest point in region of attraction in the same direction. For example, if $[\hat{z}_1, \hat{z}_2, \hat{z}_3]^T = [0, 1.5, 0]^T$, then it is pulled to $[\hat{z}_1, \hat{z}_2, \hat{z}_3]^T = [0, 1, 0]^T$. Since we use a proportional gain controller in z-space, this pull-back affects only the magnitude of the input and not the sign of the input.

We tested our controller over a uniform grid ($10 \times 10 \times 10$) of 1000 initial conditions of up to ± 10 mm error in depth from the plane, and up to $\pm 15^\circ$ initial error in both "pitch" and "roll" (x_2 and x_3). In all cases, we seeded the initial condition of the observer to $\hat{z}_2 = \hat{z}_3 = 0^\circ$, and for the first state, $\hat{z}_1 = z_1 + \ noise$ of up to 1 mm. Each initial condition was simulated 10 times with noise, for a total of 10,000 simulations. Each insertion was to a length of 30 cm. We found that:

- 93% of initial conditions converged to within ± 6 mm.
- 75% of initial conditions converged to within ± 3 mm.
- even when the states did not converge within the ± 6 mm tolerance, they did not "blow up" (*i.e.* the states did not diverge to infinity).

Next, we tested our controller with initial conditions of up to ± 10 mm error in depth from the plane, and up to

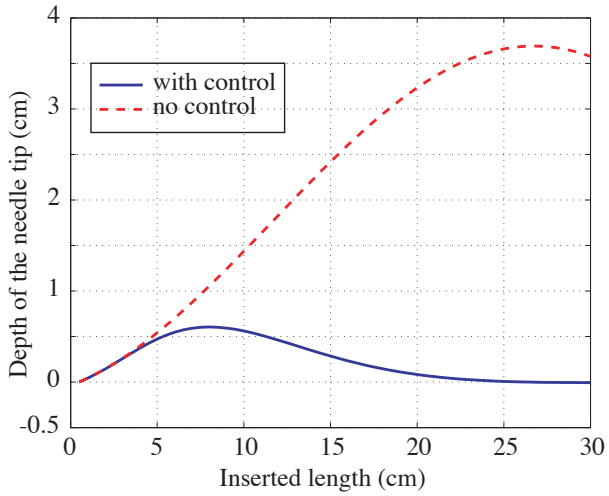

Fig. 4. Simulation with an initial deviation of $\beta = 5°$ and $\gamma = 10°$ and correct depth. In this simulation there is no measurement noise. With no control, even when the needle starts on the desired plane, small deviations in the "pitch" and "roll" cause the needle to diverge the needle from the desired plane. With control, the needle stabilizes to the desired plane.

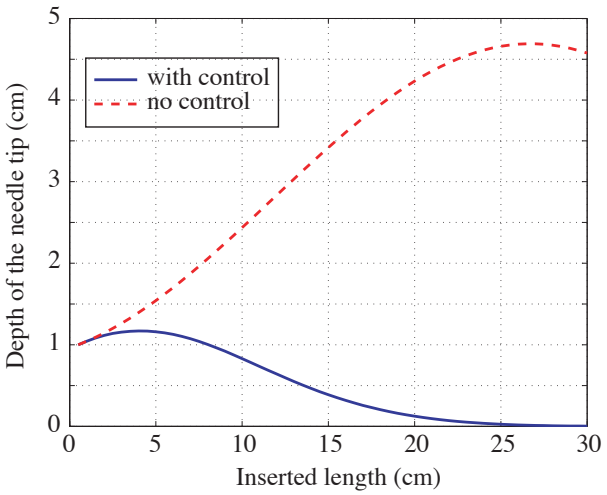

Fig. 5. Simulation with initial deviation of $x_1 = 10mm$, $\beta = 5°$ and $\gamma = 10°$. In this simulation there is no measurement noise. With no control, the needle very does not converge to the desired plane. With control, the needle stabilizes to the desired plane.

$\pm 10°$ initial error in both "pitch" and "roll" (x_2 and x_3) and insertion length of 30 cm. We found that:

- 99% of initial conditions converged to within ± 6 mm.
- 80% of initial conditions converged to within ± 3 mm.
- even when the states did not converge within the ± 6 mm tolerance, they did not "blow up".

Using an initial condition of $\mathbf{x}_0 = [10\text{mm}, 3°, 5°]^T$, we tested the controller using an incorrect value of κ (up to 20% error) and found that the controller always converged. Thus the system appeared to be insensitive to parametric uncertainty; an analytic proof of this remains a work in progress.

B. Characteristic Examples

We show a few characteristic examples to give the reader a flavour of the controller. In these simulations, the model parameter was taken as $1/\kappa = 9.7\ cm$. In the first example, initial conditions have the correct depth but non-zero (and unknown) pitch and roll. Such initial conditions are typical in physical experiments for testing 2D path planners. An example simulation with no noise measurement is shown in Figure 4. In the next few examples, we navigate the needle to a desired plane in the tissue far away from its initial entry point (Figures 5, 6, 7). In these plots, the x-axis is the length of needle inserted into the tissue and the y-axis is the depth (distance) of the needle tip away from the $y-z$ plane. Recall that, at the goal depth is zero. In all these examples, we can observe that the controller stabilizes the needle tip to the desired plane, while without any control, the needle tip never converges to the desired plane.

C. Exploratory Laboratory Experiments

Preliminary experiments were also conducted on the needle steering device described in Section II. In this apparatus, two stereo cameras track the three-dimensional position of

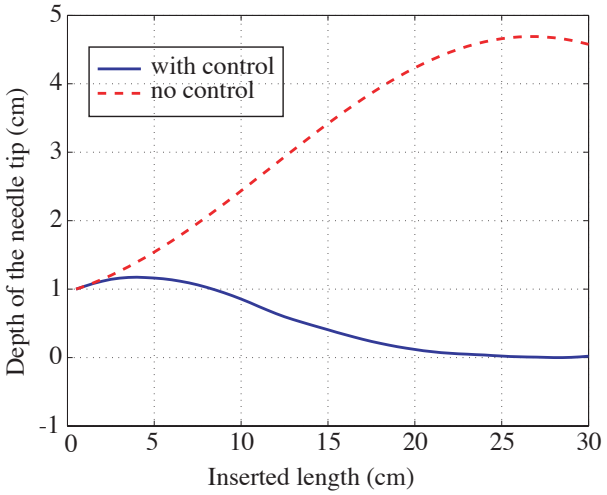

Fig. 6. With measurement noise: Simulation with insertion speed of 0.5cm/s and a deviation of $x_1 = 10mm$, $\beta = 3°$ and $\gamma = 5°$. Noise in the depth measurement is within $\pm$1mm.

a needle tip. The gel used in the experiments is about 35mm thick, so that it is sufficiently transparent for tracking purposes. This phantom tissue has a refractive index of about 1.3. Refraction is accounted for in our calculations by assuming that tissue's top surface is horizontal. Due to this assumption, we notice an error of about 4 mm in position estimates, much higher than one expects from fluoroscopy and ultrasound (0.8 mm). The needle used for the experiments had a radius of curvature of 9.7 cm when inserted into the tissue. Figure 8 shows our two best trials to date obtained in laboratory experiments.

Since measurement noise was very high in our present experimental setup, we noticed that our region of attraction was very small despite carefully tuned controller gains. We believe that with ultrasound or fluoroscopy the controller will

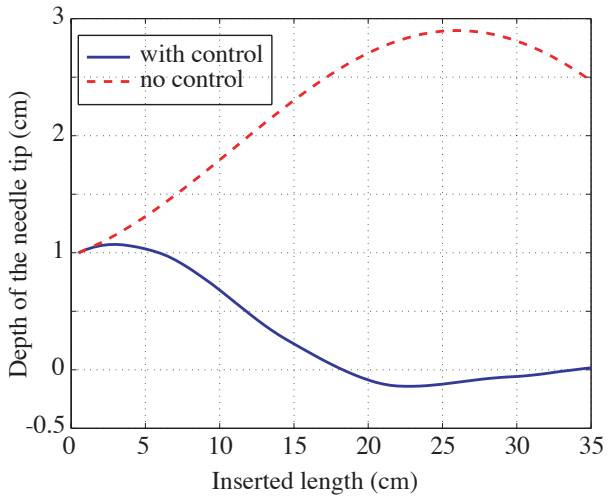

Fig. 7. Error in the parameter value: Initial deviation of $x_1 = 10mm$, $\beta = 3^\circ$ and $\gamma = 5^\circ$. Error in the parameter value is 10%. Noise in the depth measurement taken to be within $\pm$1mm. Notice that the controller stabilizes the needle tip to the desired location even when there is an error in the model parameter, κ.

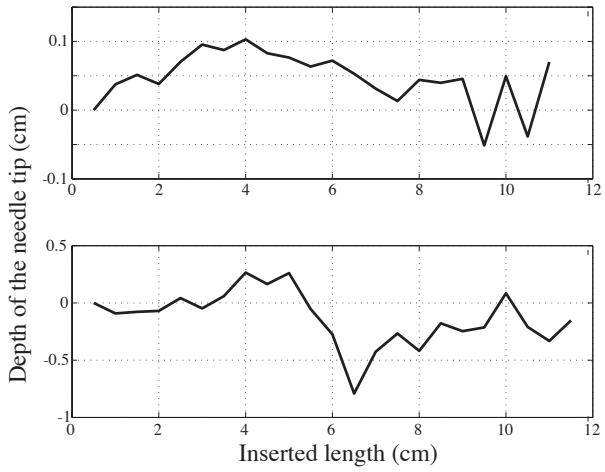

Fig. 8. Experimental runs with needle inserted at the right depth: We cannot accurately determine the initial values of other two states- x_2 and x_3 during the initial insertion. With the controller the distance of the needle tip from the desired 2D plane is within the measurement noise levels.

work much better, as can be seen in the simulations. We are currently working to enhance the visual tracking setup to enable measurements with lower noise.

VI. Discussion and Future Work

We present a nonlinear observer-controller pair that stabilizes a flexible bevel-tip needle to a desired 2D plane. By reparameterizing the kinematic models as functions of arc length, rather than time, we allow for human control of insertion speed, and our controller rotates the needle accordingly. This paradigm will enhance safety by keeping the surgeon in the loop in a manner that enables him or her to regulate the insertion speed while monitoring the progress of corrective steering actions.

Our next step is to evaluate the performance of this controller by conducting tests on a variety of tissues (phantom, *ex vivo*, and animal cadaver) using ultrasound or fluoro imaging systems. Due to tissue inhomogeneity, implementing control on real tissue might benefit from an adaptive version of our controller that would "learn" the model parameters while stabilizing the needle to a 2D plane. Our ultimate goal is to incorporate automatic needle steering with pre- and intra-operative planning to greatly enhance the effectiveness of percutaneous therapies.

VII. Acknowledgements

This work is supported in part by National Institutes of Health grant R21-EB003452. The authors thank Allison Okamura for the ideas that helped start this work, Robert Webster for building the needle insertion device, Katie Zhuang, Robinson Seda-Padilla and Joe Romano for help in making flexible bevel-tip needles and phantom tissue. Eatai Roth and John Swensen provided critical review of the manuscript.

References

[1] R. Alterovitz, K. Goldberg, and A. Okamura. Planning for steerable bevel-tip needle insertion through 2D soft tissue with obstacles. *IEEE International Conference on Robotics and Automation,*, pages 1652–1657, 2005.

[2] F. Azar, D. Metaxas, and M. Schnall. A finite element model of a finite element of the breast for predicting mechanical deformations during biopsy procedures. *Workshop Mathematical Methods in Biomedical Image Analysis*, pages 38–45, 2000.

[3] S. DiMaio, G. Fischer, S. Haker, N. Hata, I. Iordachita, C. Tempany, R. Kikinis, and G. Fichtinger. A system for MRI-guided prostate interventions. *International Conference on Biomedical Robotics and Biomechatronics*, 2006. in press.

[4] S. DiMaio and S. Salcudean. Needle insertion modeling and simulation. *Transactions on Robotics and Automation*, 19:864–875, 2003.

[5] S. DiMaio and S. Salcudean. Needle steering and model-based trajectory planning. *Medical Image Computing and ComputerAssisted Intervention*, pages 33–40, 2003.

[6] M. Ding and H. N. Cardinal. Automatic needle segmentation in three-dimensional ultrasound image using two orthogonal two-dimensional image projections. *Medical Physics*, 30(2):222–34, 2003.

[7] J. Engh, G. Podnar, S. Khoo, and C. Riviere. Flexible needle steering system for percutaneous access to deep zones of the brain. *IEEE Northeast Bioengineering Conference*, 2006.

[8] J. Engh, G. Podnar, D. Kondziolka, and C. Riviere. Toward effective needle steering in brain tissue. *International Conference of the IEEE Engineering in Medicine and Biology Society*, 2006.

[9] D. Glozman and M. Shoham. Flexible needle steering and optimal trajectory planning for percutaneous therapies. *Medical Image Computing and Computer-Assisted Intervention - MICCAI*, pages 137–144, 2004.

[10] H. K. Khalil. *Nonlinear Systems*. Prentice Hall, 2 edition, 2002.

[11] S. Nath, Z. Chen, N. Yue, S. Trumpore, and R. Peschel. Dosimetric effects of needle divergence in prostate seed implant using I and Pd radioactive seeds. *Medical Physics*, 27:1058–1066, May 2000.

[12] W. Park, J. S. Kim, Y. Zhou, N. J. Cowan, A. M. Okamura, and G. S. Chirikjian. Diffusion-based motion planning for a nonholonomic flexible needle model. In *IEEE International Conference on Robotics and Automation*, pages 4600–4605, Barcelona, Spain, April 2005. IEEE.

[13] R. J. Webster, N. J. Cowan, G. S. Chirikjian, and A. M. Okamura. Nonholonomic modeling of needle steering. *International Journal of Robotics Research*, 25(5/6):509–526, May/June 2006.